Journal of Pharmaceutical Innovation (2025) 20:163
https://doi.org/10.1007/s12247-025-10064-x

RESEARCH

Mimosa pudica Linn. Root Extract-Mediated Synthesis of Zinc Oxide Nanoparticles: a Study of Glucose Uptake Efficiency on 3T3-L1 Adipocytes

Chandrasekar Palanichamy[1] · Pavadai Parasuraman[2] · Panneerselvam Theivendren[3] · Murugesan Sankaranarayanan[4] · Madasamy Sundar[5] · Selvaraj Kunjiappan[6]

Accepted: 27 July 2025

Abstract

Purpose *Mimosa pudica* is a medicinal plant conventionally used to cure various ailments, including diabetes and is a model for synthesizing new drug derivatives. This work evaluates the glucose utilization potential of Zinc oxide nanoparticles (ZnONPs) derived from the ethanol root extract of *M. pudica* in 3T3-L1 adipocyte cells.

Methods Molecular modeling tools were used to predict the potential antidiabetic compounds from *M. pudica*. ZnONPs were biosynthesized using *M. pudica* extract, and their physicochemical properties were characterized using UV-visible, FTIR, XRD, DLS, XPS, and FESEM techniques. The in vitro cellular viability of synthesized ZnONPs and glucose utilization efficiency were examined in 3T3-L1 adipocytes.

Results Using GC-MS and LC-MS analyses, 27 novel bioactive compounds were identified from *M. pudica* root extract. For the efficient glucose utilization in 3T3-L1 adipocytes, Dipeptidyl-peptidase 4 (DPP-4) inhibition plays a pivotal role, as three of the top binding-scored molecules from *M. pudica* were identified via molecular docking and dynamics simulation studies. 500 µg of ZnONPs exhibited 73.47 ± 1.59% cellular viability. Further, the in vitro glucose utilization efficiency of ZnONPs was evidenced in 3T3-L1 adipocytes, which displayed concentration-dependent glucose utilization. The effect of ZnONPs (30 µg) on glucose uptake was higher than that of 10 µg of metformin. Bioactive compounds from *M. pudica* extract might inactivate the DPP-4 enzyme activity and improve insulin release from the pancreas, lowering blood glucose levels via GLUT4 activation.

Conclusion The findings imply that *M. pudica*-mediated synthesized ZnONPs might be a plant-based novel oral nanoformulation for managing diabetes mellitus (DM).

Selvaraj Kunjiappan
selvaraj.k@sethu.ac.in

Chandrasekar Palanichamy
p.chandrasekar@klu.ac.in

Pavadai Parasuraman
pvpram@gmail.com

Panneerselvam Theivendren
tpsphc@gmail.com

Murugesan Sankaranarayanan
murugesan@pilani.bits-pilani.ac.in

Madasamy Sundar
sundarcrpb@gmail.com

[1] Kalasalingam Academy of Research and Education, Krishnankoil, India

[2] M.S. Ramaiah University of Applied Sciences, Bengaluru, India

[3] Vels Institute of Science, Technology & Advanced Studies, Pallavaram, Chennai, India

[4] Birla Institute of Technology & Science Pilani, Pilani, India

[5] Department of Biotechnology, Bharathidasan University, Tiruchirappalli, India

[6] Department of Biotechnology, Sethu Institute of Technology, Kariapatti, India

Published online: 09 August 2025

Statement of Novelty

- ZnONPs are among the most extensively studied inorganic nanoparticles and are an excellent option for therapeutic applications due to their low toxicity and biocompatibility.
- Biosynthesis of metal nanoparticles through plant-derived phytocompounds is more efficient than other natural sources.
- Interestingly, M. pudica extract-mediated synthesized ZnONPs did not cause any toxicity to 3T3-L1 adipocytes.
- ZnONPs enhanced the glucose utilization efficiency in 3T3-L1 adipocytes.

Graphical Abstract

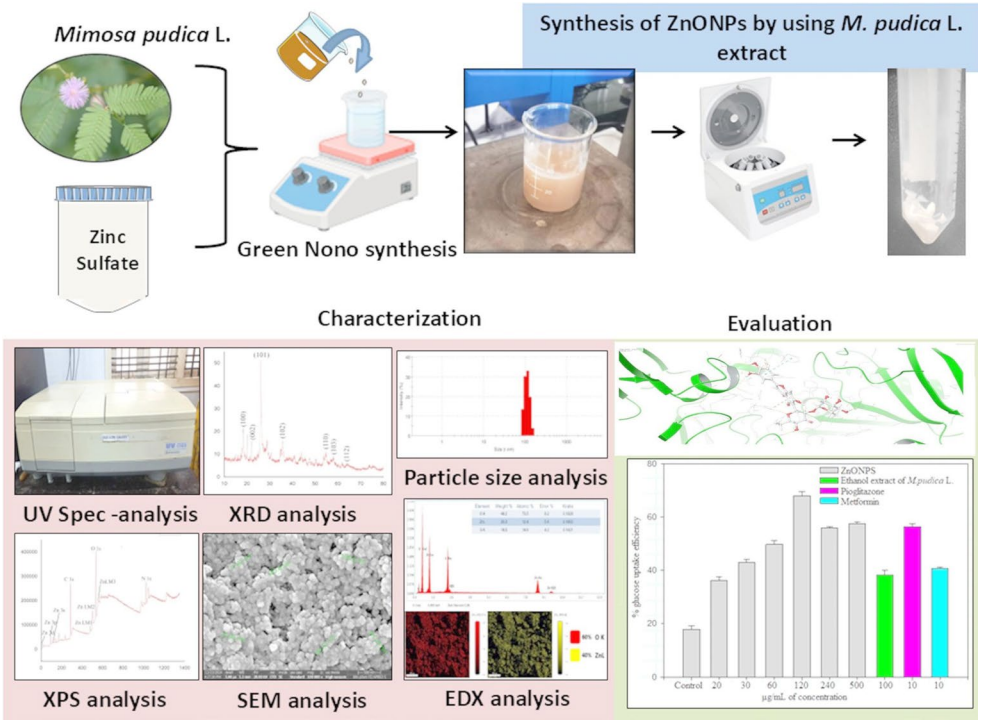

Keywords Diabetes mellitus · 3T3-L1 adipocytes · Glucose utilization · *Mimosa pudica* Linn. · Molecular dynamics simulation

Introduction

Hyperglycemia is a chronic metabolic illness marked by elevated blood glucose levels due to insufficient insulin synthesis (type 1 DM), impaired utilization (type 2 DM), or a combination of both [1]. Diabetes is the second most common disease, affecting 25% of the global population [2]. Every two years, the International Diabetes Federation (IDF) announces reports that the number of people affected by diabetes increases, with new cases, from 200 million in 1990 to 830 million by 2022 [3]. The prevalence has escalated more rapidly in low- and middle-income countries than high-income nations [4]. Type 2 Diabetes Mellitus (T2DM) is defined by inadequate insulin production in pancreatic β-cells and insulin resistance in target tissues. Insulin resistance is the pathophysiological basis of T2DM, occurring when muscle cells, adipocytes, and the liver fail to respond to insulin and cannot ingest glucose from the bloodstream [5]. The pancreas secretes increased insulin to facilitate glucose entry into muscle and liver cells, while adipose tissue significantly contributes to energy homeostasis by modulating insulin-mediated glucose uptake [6]. The insulin-sensitive glucose transporter (GLUT4) facilitates glucose transfer in adipose tissue by oscillating between intracellular storage vesicles and the plasma membrane; any disruption in GLUT4 translocation restricts glucose uptake, ultimately resulting in insulin resistance [7]. In T2DM, insulin fails to adequately execute glucose metabolism, producing a high glucose level in the liver via glucagon [8]. Most synthetic antidiabetic drugs have adverse effects and should not be used during pregnancy [9]. However, they were unable to cure the diabetic condition completely. Although various medicines can manage and maintain normal blood sugar levels, no single treatment can cure this disease. As a result, it is promising to design new therapies for T2DM that

increase insulin activity while decreasing/inhibiting glucagon activity, which will be a massive challenge for modern science.

Insulin resistance and obesity were significantly correlated in obese patients exhibiting pronounced lipolysis, resulting in elevated free fatty acid concentrations in the bloodstream [10]. Increased free fatty acid concentrations can inhibit insulin binding to its receptors by diminishing the quantity of insulin receptors on the membranes of insulin-sensitive organs [11]. DPP-4 (Dipeptidyl-peptidase 4) is an exopeptidase in serum and on the surfaces of several cell types, such as adipocytes, monocytes, lymphocytes, and endothelial cells [12]. DPP-4 cleaves and inactivates a variety of substrates, including the incretins glucose-dependent insulinotropic polypeptide (GIP) and glucagon-like peptide-1 (GLP-1), as well as several other peptides and cytokines [13]. Incretins, GIP, and GLP-1, which reduce glucose levels in the stomach, account for 50–70% of total insulin generated after oral glucose delivery [14]. A high-fat diet (HFD) was found to have the reverse effect on incretin levels, boosting GIP levels and lowering GLP-1 secretion [15]. Adipose tissue is a known GIP target, with GIP receptor (GIPR) levels rising as adipocytes mature, despite producing both GIP and GLP-1 receptors. GIP may contribute to fat accumulation because it mediates several anabolic effects in adipose tissue, including increasing glucose uptake, upregulating the expression of lipoprotein lipase (LPL) and the lipogenesis enzyme fatty acid synthase (FAS), and reducing glucagon-induced lipolysis [16]. Furthermore, multiple studies have found that downregulating DPP-4 and their signaling pathways may be a checkpoint for developing new drugs to treat obesity and T2DM [17–19].

Numerous techniques, such as nanoparticulate systems, are being investigated as prospective alternatives for current T2DM treatments to improve pharmacological efficacy. Zinc oxide nanoparticles (ZnONPs) have sparked interest since zinc has a variety of applications, including treating diabetes, promoting insulin synthesis, improving antioxidant enzyme activity, reducing inflammation, and increasing hepatocyte activity [20–24]. Physical, chemical, or biological mechanisms are frequently used to create ZnONPs. Toxic substances with potentially harmful effects, high energy requirements, high costs, and time-consuming operations are some disadvantages of physical and chemical techniques [25]. Biological techniques for nanoparticle synthesis include the use of microbial and plant extracts. Because plants are widely available, employing plant extracts, also known as "green synthesis," is simple, needs fewer steps, is less expensive, and is particularly appealing. Using the green synthesis process reduces the generation of harmful byproducts and reduces the need for toxic solvents or chemical agents, which are commonly required in traditional synthesis procedures. Their reducing, antioxidant, or antidiabetic phytocompounds (such as phenolics) increase ZnONPs synthesis, adhere to their surface, and may improve their activity by lowering ROS (reactive oxygen species) levels and, as a result, the harm caused by hyperglycemia [20].

Many medicinal plants have been explored to find the therapeutic bioactive compounds which can remedy diabetic disorders, but there have been limited studies examining the ameliorative purposes of creeping herbs. According to the information, *Mimosa pudica* Linn. (Family: Fabaceae) is a sub-woody plant native to South America and may also be found in Australia and India. It could be either annually or biannually [26]. Traditionally, *M. pudica* crude extract has been applied to cure various conditions, including metabolic and heart disease [27]. Extracts from *M. pudica* have been demonstrated to reduce arginine-induced acute pancreatitis. By considerably reducing glutathione depletion and hyperglycemic stress, the phytoconstituents of *M. pudica* are therapeutically effective pharmacological agents for the treatment of diabetes and its consequences, the study found [28]. Our earlier study showed that in male Wister rats with diabetes, the ethanol extract of *M. pudica* lowers blood glucose levels and encourages sexual behaviors. Consequently, *M. pudica* is an important phytocompound and drug source that prevents diabetes [27]. However, it has been shown that plant-derived compounds' molecular structure, lipid insolubility, and membrane impermeability result in low bioavailability of their bioactive components, limiting their entry into the systemic circulation [29]. This indicates that the absorption and bioavailability of any phytoconstituent derived from plants determines its beneficial properties. As a result, the researchers postulated that *M. pudica* ethanol extract-reduced ZnONPs would be an effective and appropriate formulation to overcome the structural complexity associated with poor absorption and reduced bioavailability of phytocompounds. Furthermore, nanosized *M. pudica* ethanol extract-mediated synthesized ZnONPs could be used as a simple oral medication to treat diabetes. Bioactive compounds from *M. pudica* extract might inactivate the DPP-4 enzyme and promote insulin secretion from the pancreas, reducing blood glucose levels through GLUT4 activation. The study hypothesizes that synthesizing ZnONPs using *M. pudica* ethanol extract-derived bioactive compounds may significantly interact with its therapeutic target, such as DPP-4, and enhance intracellular processes for efficient cellular glucose uptake. Before the synthesis of ZnONPs, phytocompounds from *M. pudica* were assessed by Gas chromatography-Mass spectroscopy (GC-MS) and Liquid chromatography-Mass spectroscopy (LC-MS). The size, shape, and surface charge (zeta potential) of synthesized ZnONPs were studied using field emission scanning

electron microscopy (FESEM), dynamic light scattering (DLS), and X-ray diffraction (XRD) analysis. Fourier transform infrared spectroscopy (FTIR), energy dispersive X-ray analysis (EDAX) and X-ray photoelectron spectroscopy (XPS) investigations looked into the existence of functional groups and elements in ZnONPs and their structural stability: cellular viability and glucose utilization efficiency of ZnONPs generated from *M. pudica* extract. 3T3-L1 adipocytes were also employed.

Hypothesis

The proposed mechanism of action of *M. pudica* extract-mediated ZnONPs on glucose uptake in 3T3-L1 adipocytes. GC-MS and LC-MS analysis reported that 27 bioactive compounds, such as Cassiaoccidentalin B, Isoorientin, Isoquercetin, Apigetrin, Vitexin, Orientin, Aviculin, Stigmasta-7,16-dien-3-ol, Betulinic acid, Isovitexin, 6,8-dioxabicyclo[3.2.1]octane, 4 H-pyran-4-one, Ethanamine, 5-hydroxymethylfurfural, Beta-d-Ribopyranoside, 3,4-altrosan, Imidazole, Imidazole-4-carboxylic acid, Caffeine, cis-vaccenic acid, 1-methyl-3,3-pentamethylenediazine, 2 H-azepin-2-one, 3-dibenzofuranamine, Bufadienolide, Mimopudine, Gallic acid, and Mimosine. The bioactive compounds-mediated synthesis of ZnONPs inhibits the activity of DPP-4 enzymes and leads to the breakdown of the incretins, glucose-dependent insulinotropic polypeptide (GIP), glyceraldehyde-3-phosphate (G3P), and glucagon-like peptide-1 (GLP-1). Breakdown of Incretins, GIP, G3P, and GLP-1 stimulates insulin secretion from the pancreas and reduces the glucagon level. This, in turn, helps lower blood sugar levels by facilitating glucose uptake into adipocyte cells and reducing glucose production by the liver, as represented in Fig. 1.

Experimental Section

Chemicals

Zinc sulfate, sodium hydroxide, and other chemicals used in this experiment were purchased from SRL, Pvt. Ltd., Mumbai, India, and were of research grade. 3-(4, 5-dimethyl-2-thiazolyl)-2, 5-diphenyltetrazolium bromide (MTT), insulin, L-glutamine, fetal bovine serum (FBS), streptomycin, penicillin, and Dulbecco's modified eagle's medium (DMEM) were procured from Himedia Laboratories Pvt. Ltd., Mumbai, India. 6-(N-(7-nitrobenz-2-oxa-1,3-diazol-4-yl) amino)-2-deoxyglucose (6-NBDG) and 1-isobutyl-3-methylxanthine (IBMX) were procured from Sigma-Aldrich, Bangaluru, India.

Mimosa Pudica Linn

Mimosa pudica was collected from May to June (when the plant is actively growing and has reached maturity) in Thaniparai, near the Western Ghats (Longitude: 77.6328°N; Latitude: 9.7031°E), Virudhunagar District, Tamil Nadu, India. The taxonomist validated the plant specimen. The

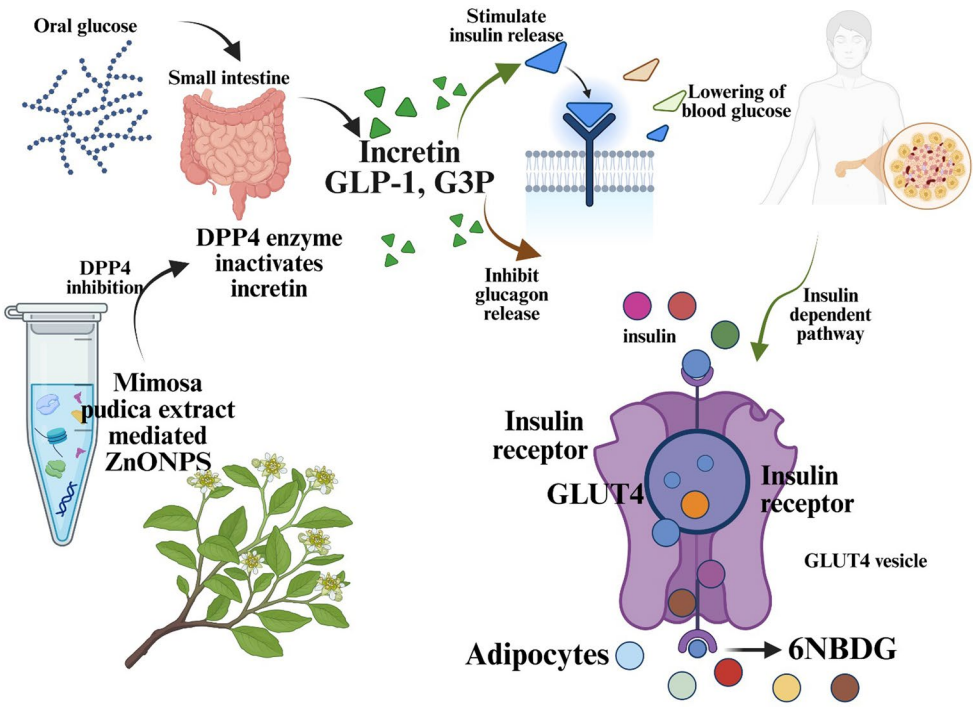

Fig. 1 Mechanism of glucose-utilization efficiency by *M. pudica* phytochemicals

entire plant was collected; no regulation was required for the collection of this plant. The voucher (specimen number ANJAC/PAC/06) was created and submitted to the Centre for Research Postgraduate Studies in Botany at Ayya Nadar Janaki Ammal College, Sivakasi, Tamil Nadu, India. The plant root was washed with tap water, rinsed with deionized water, and air-dried at room temperature in a shaded environment for one week. The desiccated plant material was pulverized into a fine powder and preserved in an airtight plastic container for the experiment.

3T3-L1 Adipocytes

The National Centre for Cell Sciences (NCCS) in Pune, India, provided the 3T3-L1 preadipocytes, which were then cultivated in DMEM media supplemented with 10% donor calf serum and 1% L-glutamine, penicillin, and streptomycin for 24 h at 37 °C in a CO_2 incubator.

3T3-L1 Adipocytes Differentiation

The 3T3-L1 preadipocytes were cultivated to conglomerate in 12-well culture plates (60,000 cells/well) to facilitate 3T3-L1 preadipocyte differentiation [30]. The cells were treated for five days in a differentiation medium with DMEM, 10% fetal bovine serum, 0.25 mM dexamethasone, 0.5 mM IBMX, and 1 µM insulin to induce cell differentiation. Multinucleate cells were identified as well-differentiated adipocytes, and the medium was changed every two days. A standard medium containing two microgrammes of insulin per millilitre was substituted for the culture media. The cells were fed a regular medium for two more days.

Mimosa Pudica Extract

Using the ultrasound-assisted extraction approach, an extract abundant in bioactive components was obtained from powdered *M. pudica* root. The ultrasound-assisted extraction apparatus comprised a jacketed reactor with a 250 mL capacity (produced by PCI Analytics Ltd., Mumbai, India), an ultrasonic water bath featuring a temperature accuracy of ± 1.0 °C, a power supply of 220 V, and a continuous operation mode at a 20 kHz high-intensity ultrasound processor. 200 mL of 70% ethanol, 20 g of *M. pudica* (0.5 mm particle size), and further extraction parameters were subjected to sonication at a 0.4 pulse cycle, 60 W cm^{-2} ultrasound intensity, and 45 °C for 20 min. Ethanol is used for extraction due to its versatility, safety, and efficiency as a solvent, particularly for chemicals isolated from natural sources and biological applications. It can extract a broad spectrum of substances, is non-toxic mainly, and easy to recover, making it a preferred choice in the biopharmaceutical industry. After extraction, the Whatman No. 1 filter paper removed the plant powder. The resultant filtrate was evaporated at 40 °C using a rotary vacuum evaporator (Buchi, Rotavapor R-200, Mumbai, India). Following lyophilization to convert it into powder, the concentrated ethanol extract was stored in a desiccator until the experiment [31].

Screening of Bioactive Compounds Through GC-MS and LC-MS

Our previous work identified 27 bioactive components by GC-MS and LC-MS analyses from the ethanol extract of *M. pudica* root. The identified bioactive compounds are provided in the supplementary Table 1.

Molecular Docking Studies

The above-listed compounds from *M. pudica* ethanol extract were used to perform molecular docking experiments to predict potential Dipeptidyl Peptidase 4 inhibitors. DPP-4 was chosen as a target for glucose metabolism in 3T3-L1 adipocytes because it controls glucose homeostasis by degrading incretin hormones such as GLP-1 and GIP, which promote insulin release while inhibiting glucagon secretion. By inhibiting DPP-4, the levels of these incretins are elevated, resulting in better glucose management and potentially reducing insulin resistance. The selected pharmaceutical compounds were docked to the human dipeptidyl peptidase IV (DPP-4) receptor utilizing the PyRx 0.8 tool within the Auto Dock Vina program. The coordinate file and X-ray crystal structure of the DPP-4 protein dipeptidyl peptidase IV (DPP-4) complexed with prolyl thiazolidine inhibitor #1 (PDB entry ID: 3VJM, resolution 2.10 Å) are accessible through the Research Collaboratory for Structural Bioinformatics, Protein Data Bank (RCSB PDB) Website. Utilizing Swiss-PDB Viewer v4.1.0, the protein's side chain anomalies and inappropriate bonding were rectified, and absent residues were included. The file was designated as Target.pdb and preserved for future utilization. The three-dimensional structure of the detected molecule was shown using ACD/Chemsketch software (version 2021.2.2, Toronto, Ontario, Canada), and energy optimization was performed using MMFF94 [32]. The ready-to-dock library was developed utilizing the BIOVIA Discovery Studio software. The inhibitory effects of the discovered compounds were compared to prolyl thiazolidine, a prevalent DPP-4 inhibitor (PubChem CID: 70047390). The identified ligands were transformed into the ".pdbqt" file format utilizing the Open Babel tool (https://openbabel.org/) following energy minimization with the Avogadro tool (https://avogadro.cc/).

Molecular Dynamics Studies

The complex, time-dependent evolution was performed over 100 ns using the Desmond dynamic package 2017 in Schrodinger (academic version) running under Linux. Potential binding and the interactions of the PLC (protein-ligand complex) present at the target site in a physiological environment, training of MD simulation was performed (Schrodinger, LLC; Schrodinger Release: QikProp). The panel of the system developer: The panel formed a water-filled $10 \times 10 \times 10$ box, including physiological parameters such as pH. In the absence of pH when it needs to be increased or lowered to meet the requirements of study methodology, Na^+ or Cl^- ions can be added. We used the simple orthorhombic point charge (SPC) water model to solve the docked protein-ligand complexes. The solvated system was neutralized with counter ions, and the physiological salt concentration was 0.15 M. The OPLS AA (Optimal Potentials for Liquid Simulation-All Atom) force field was used for the PLC system. The system builder panel minimizes (200 picoseconds) the ready PLC. Molecular dynamics was performed using a Nose-Hoover chain thermostat, a Martyna-Tobias-Klein barostat, and the integrator of the Reversible Reference System Propagator Algorithms (RESPA), with two picosecond relaxation times [33]. A final iteration of the MD simulation was run on the equilibrated system. Thus, the MD was continued for 100 ns at 310.15 K and 1.0 bar pressure through NPT (Isothermal-Isobaric ensemble; constant temperature, constant pressure, and constant number of particles) ensemble by default relaxation parameters. After the simulation, results were analyzed using a simulation interaction diagram [34].

Synthesis of *Mimosa Pudica* L. extract-mediated Zinc Oxide Nanoparticles

In a conical flask, 50 mL of 0.02 mol/L Zinc sulfate solution was mixed with 100 mg of freeze-dried *M. pudica* root extract powder in 20 mL of deionized water for an environmentally friendly synthesis of the ZnONPs. The mixture was then incubated for 1.5 h in a magnetic stirrer. Later, to bring the mixture's pH down to 7, 0.2 mol/L of NaOH solution was gradually added. The liquid was magnetically stirred. The zinc oxide nanoparticles were centrifuged for 5 min at 4000 rpm following the reaction. After discarding the supernatant, the precipitates underwent two water washes and were lyophilized (freeze-dried) [35].

ZnONPs Characterization Studies

A notable color change was observed after incubating the ethanol root extract of *M. pudica* with Zinc sulfate solution. UV-visible Spectroscopy (Shimadzu UV-2700, Kyoto, Japan) was used to confirm the peak of synthesized ZnONPs using ethanol root extract of *M. pudica* within the wavelength range from 200 to 800 nm. The characteristic peak confirming the formation of ZnONPs was observed [36]. The lyophilized powder of ZnONPs was further used for various analyses such as FTIR, XRD, FESEM-EDX, and XPS. The FTIR spectrum (IR Spirit-X series, Shimadzu, Kyoto, Japan) is a reliable method for identifying phytoconstituents and functional groups that facilitate the stabilization and reduction of ZnONPs within the range of 400–4000 cm^{-1}. A small (approximately 1 mg) amount of finely powdered lyophilized ZnONPs was mixed with infrared (IR) grade potassium bromide (KBr) to obtain a round disc (with the help of a hydraulic press) suitable for FTIR measurement [37]. Field emission scanning electron microscopy (FESEM) analysis, a solution of a ZnONPs sample was placed on a carbon strip attached to an FESEM brass, extra solution was wiped using blotting paper and then allowed to dry by putting it under a mercury lamp for 5 min. Field emission scanning electron microscopy (FESEM) (Apreo 2 Thermo Scientific, Waltham, MA, USA), coupled with an X-ray fluorescence spectrometer (Oxford INCA X-max 80) for energy dispersive X-ray analysis (EDAX), and the XRD measurement was carried out on thoroughly dried thin films of the purified lyophilized ZnONPs powder on a glass slab of a X-ray diffraction (XRD) (Rigaku SmartLab 9, Tokyo, Japan) utilizing Cu-Kα radiation at 40 kV and 40 mA, were employed to examine the surface morphology, elemental composition, dimensions, and morphology of green synthesized Zinc Oxide nanoparticles (ZnONPs). The surface elemental composition of ZnONPs was analyzed using X-ray photoelectron spectroscopy (XPS) using a VersaProbe III Scanning XPS Microprobe spectrometer (Physical Electronics, Chanhassen, MN, USA) and an aluminium Kα X-ray source at a photon energy of 1486.6 eV. The zeta potential, polydispersity index (PDI), and mean particle size of the freshly synthesized solution of ZnONPs were assessed using a Zetasizer Nano ZS ver.7.03 (Malvern Instruments, Malvern, Worcestershire, United Kingdom) [38].

Cellular Viability Study Through MTT Assay

The MTT assay assessed the cellular viability of ZnONPs mediated by ethanol extract against 3T3-L1 adipocytes at varying concentrations of ZnONPs (20, 30, 60, 120, 240, and 500 µg/mL) [39]. The MTT assay is the predominant technique for evaluating cellular metabolic activity. The cellular mitochondrial dehydrogenase enzyme's capacity to break the yellow, water-soluble MTT, resulting in insoluble dark blue/purple formazan deposits in living cells, renders it a dependable colorimetric and quantitative assay. A 96-well

tissue culture plate was used to seed 1×10^5 cells/mL (100 µL/well) of 3T3-L1 adipocytes and incubated for 24 h at 37 °C. The growth medium was removed after 24 h. After two dilutions, the sample under scrutiny was maintained in an RPMI medium supplemented with 2% serum. Three control wells were administered just serum; the others were allocated 0.1 mL of each dilution. The plate was analyzed after incubation at 37 °C. The viability of cells was examined. MTT (5 mg/mL in PBS) was formulated as a solution. 8–20 µL of MTT solution was introduced into each well, agitated vigorously for 5 min, and incubated for 4 h at 37 °C with 5% CO_2 until formazan formed. Formazan was resuspended in 200 µL of DMSO and stirred vigorously for 5 min. Absorbance was quantified at 560 nm. Three replicates of the experiment were performed. The following formula was used to determine the percentage of cell viability:

Cellular viability (%) $= A_t/A_c = 100$,

A_t and A_c are the mean absorbance of ZnONPs-treated and control cells, respectively ($n = 3$, where n is the number of independent experiments).

Glucose Utilization Studies

An enzymatic fluorometric assay detected glucose uptake using 6-NBDG uptake with minor modifications [40]. A 24-well plate containing insulin and serum-starved DMEM was utilized for culturing fully differentiated 3T3-L1 adipocyte cells (1×10^5 cells/well) for 24 h. Subsequently, the cells were administered 200 µL of differentiation media comprising various concentrations of ZnONPs (20, 30, 60, 120, 240, and 500 µg), along with standard pharmaceuticals, including pioglitazone (10 µg), metformin (10 µg), and *M. pudica* extract (100 µg) for an additional 24 h. The treated cells were thoroughly washed with ice-cold phosphate-buffered saline after being stimulated with 10 µM insulin for 15 min to terminate the reaction. Following this, 100 µL of 20 µM 6-NBDG was introduced to the treated cells and incubated for 30 min. Finally, the cells were washed and lysed using 0.5 N NaOH/0.1% SDS. After adding 30 µL of DMSO to the lysed cells, fluorescence was measured using a microplate reader with excitation and emission wavelengths of 466 and 540 nm, respectively.

Statistical Analysis

Quantitative results were presented as mean ± standard deviation (SD), and all experiments were conducted in triplicate. The data analysis and visualization were conducted using SPSS Statistics version 20.0 software (SPSS Inc., Chicago, IL, USA). Dunnett's multiple comparison test and one-way ANOVA were employed. All statistical analyses were performed with a confidence level of $p < 0.05$ to determine statistical significance.

Results and Discussion

Molecular Docking Studies

A molecular docking study determined the binding affinity and interaction of bioactive compounds obtained from the GC-MS and LC-MS analysis of *M. pudica* L. with the target protein DPP-4 (PDB ID: 3VJM). According to the docking results, all the selected compounds showed favourable binding affinities toward DPP-4, with scores ranging between −9.34 and −4.38 kcal/mol. The data of the co-crystal ligand and the top 10 compounds are shown in Table 1. The compound with the highest binding affinity was Cassiaoccidentalin B among the docked compounds, followed by Isoorientin, Isoquercetin and Apigetrin. These findings suggest that these compounds may have potent inhibitory potential against DPP-4. The docking score for the co-crystallized ligand (control) was −8.74 kcal/mol, signifying that several test compounds showed better or equivalent binding affinity than the reference ligand. For all the docked compounds, the interactions with DPP-4 included H-bonding, Pi-Pi stacking and Pi-cation interactions, which are crucial for ligand binding. Cassiaoccidentalin B formed H-bonds and Pi-Pi interactions with critical residues GLU 205, GLU 206, ARG 125, HIS 740, TYR 547 and PHE 357, implying strong binding stability. Isoorientin was primarily H-bonded with GLU 205, TYR 547, TYR 456, ASP 556 and GLN 553, denoting significant interaction with critical binding site residues. For Isoquercetin, hydrogen bonding and Pi-Pi stacking were observed with residues ARG 669, GLU 206, SER 209, TYR547, HIS 740, TYR 666 and ARG 125, which are known to be involved in DPP-4 inhibition. The interaction of Vitexin and Orientin with DPP-4 was established through hydrogen bonding and Pi-Pi interactions involving residues ARG 125, GLU 205 and GLU 206. The co-crystal ligand showed a docking score of -8.74 kcal/mol and interacted with GLU 205 and PHE 357 through hydrogen bonding and Pi-Pi interactions, as shown in Fig. 2. Of the three, Cassiaoccidentalin B, Isoorientin, and Isoquercetin had better-docked scores, implying their strong potential as DPP-4 inhibitors. These compounds exhibited more interactions than were recorded for the co-crystal ligand, thus enhancing their binding stability.

Molecular Dynamics Simulation

Based on the molecular docking analysis, the top-three binding scored ligands with DPP-4 protein

Table 1 Top-scored 10 compounds against DPP-4 and their amino acid interactions between ligands and DPP-4

S. No	Compound name	Docking Score (Kcal/mol)	Amino acid residues	Type of interactions
1	Cassiaoccidentalin B	-9.34	GLU 205, GLU206, ARG125, HIP740, TYR547, PHE357	H-bond, Pi-Pi, Pi-cation interactions
2	Isoorientin	-9.19	GLU205, TYR547, TYR456, ASP556, GLN553	H-bond interactions
3	Isoquercetin	-8.81	ARG669, GLH206, SER209, TYR547, HIS740, TYR666, ARG125	H-bond, Pi-Pi interactions
4	Apigetrin	-8.79	TYR662, PHE357, ARG125	H-bond, Pi-Pi interactions
5	Co-crystal	-8.74	GLU 205 PHE357	H-bond Pi-Pi interaction
6	Vitexin	-8.72	TYR585, CYS551, TYR547, ARG125, GLU205, GLU206	H-bond, Pi-Pi interactions
7	Orientin	-8.62	GLU206, TYR585, CYS551, TYR547, ARG125	H-bond, Pi-Pi interactions
8	Avicularin	-8.37	GLU206, PHE357	H-bond, Pi-Pi interactions
9	Stigmasterol	-8.22	GLN553	H-bond interaction
10	Betulinic Acid	-8.2	GLU205, GLU206, PHE357, ARG125, HIP740, TYR547	H-bond, Pi-Pi, Pi-cation interactions
11	Isovitexin	-8.13	GLU205, GLU206, TYR547, GLN553, TYR456	H-bond interactions

complexes, Cassiaoccidentalin B (-9.34 kcal/mol), Isoorientin (-9.19 kcal/mol), and isoquercetin (-8.81 kcal/mol), were selected for further molecular dynamics simulation studies using the DESMOND tool for 100 ns. The selection of the above three ligands is not only for binding score but also for amino acid interactions in the target protein. The Root Mean Square Deviation (RMSD) analysis gives an idea of the stability of the protein-ligand complex over the 100 ns simulation. The protein backbone RMSD was stable within an acceptable range for all three ligands, Cassiaoccidentalin B, Isoorientin and Isoquercetin, indicating that the protein remained intact. For Cassiaoccidentalin B, the RMSD initially showed slight fluctuations and then stabilized around 2.5 Å after 20 ns, which means sustained binding interaction. The ligand induces similar stability as Isoorientin and Isoquercetin, with RMSD values stabilizing at approximately 2.3 Å and 2.6 Å, respectively. From these observations regarding ligand RMSD values, it can be concluded that all three ligands were secured in the binding pocket with very minute fluctuation values, signifying strong interactions with the target protein (Figs. 3(a)-3(c)). Root Mean Square Fluctuation (RMSF) analysis was carried out to assess the flexibility of individual residues within the protein structure. The fluctuations were observed primarily at the N- and C-terminal regions, which is expected due to their inherent flexibility. Moderates fluctuate in loop regions while secondary structural elements, α-helices and β-sheets remain stable. Of all the ligands, Cassiaoccidentalin B showed slightly higher fluctuation in residues surrounding the active site. However, such variations did not affect the stability of the binding interaction. Isoorientin and Isoquercetin exhibited similar RMSF patterns with pronounced stability in the central areas of the protein (Figs. 3(d)-3(f)). The analysis of the protein-ligand interaction showed that all three ligands maintained consistent interactions throughout the simulation. Cassiaoccidentalin B had the highest number of hydrogen bonds and hydrophobic interactions, indicating a strong binding affinity. Isoorientin and Isoquercetin also exhibited stable hydrogen bonds and hydrophobic contacts, but to a slightly lesser extent. The water-mediated interactions were critical in helping the ligands bind stably in the binding pocket, which was responsible for their sustained binding during the simulation (Figs. 3(g)-3(i)). The trajectory analysis of protein-ligand interactions confirmed that all three compounds have significant potential for DPP-4 inhibition. Detailed mapping of ligand-protein interactions revealed constant engagement of critical amino acid residues involved in the binding process with the ligands. For instance, Cassiaoccidentalin B displayed interactions with critical residues for DPP-4 inhibition, namely SER 630, GLU 205 and PHE 357 (Figs. 3(j)-3(l)). Stable interactions with these residues were also observed for Isoorientin and Isoquercetin, thus confirming their binding potential. The timeline representation of interactions showed that these contacts persisted throughout the 100 ns simulation run, reinforcing these bioactive compounds' stability and

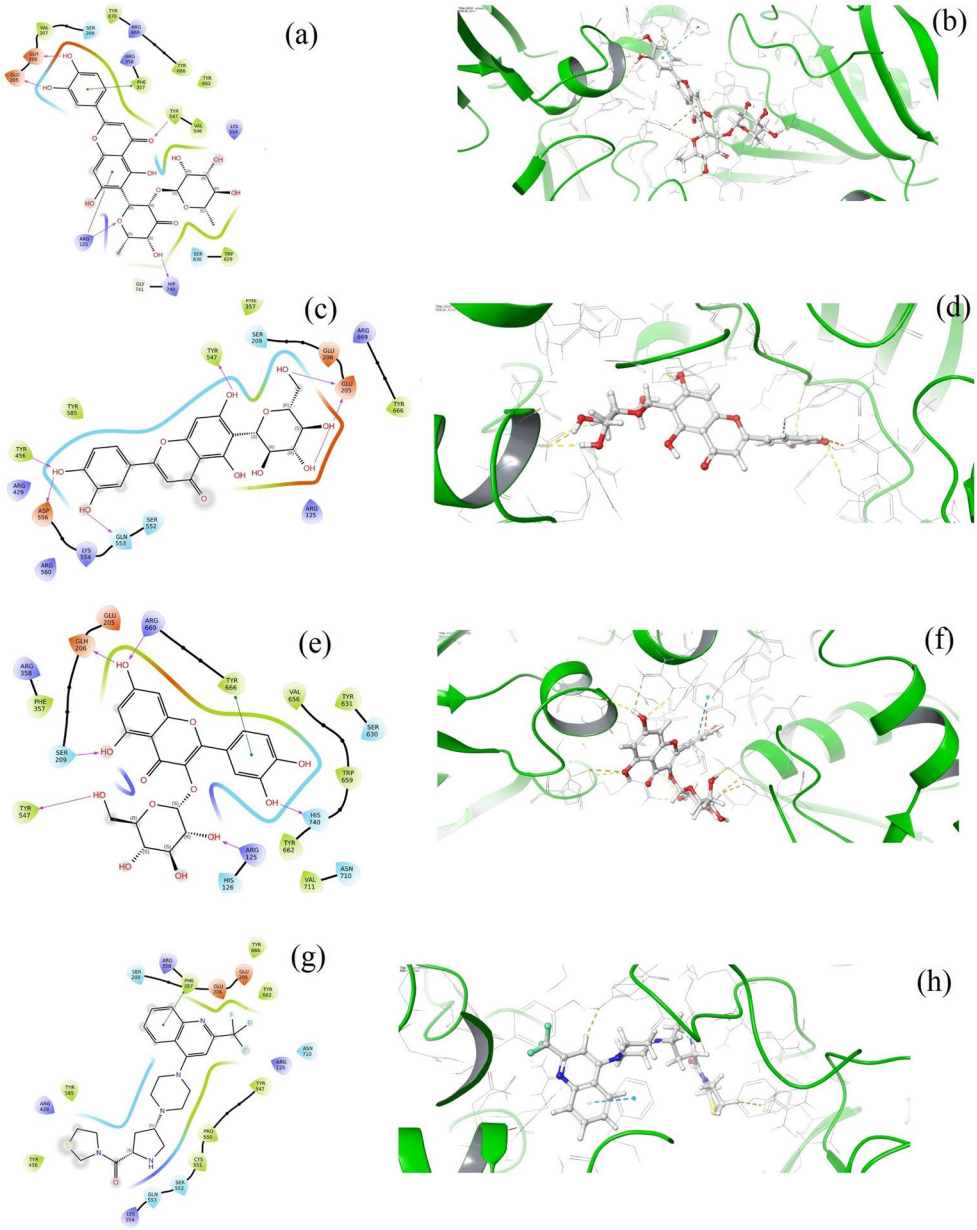

Fig. 2 Represents the interaction between the ligand and the receptor. The left side represents the two-dimensional (2D) aspect, while the right represents the three-dimensional (3D) complex protein-ligand interaction. Interaction of compounds cassiaoccidentalin B and DPP-4 (**a**, **b**); the interaction of compounds isoorientin and DPP-4 (**c**, **d**); the interaction of compounds Isoquercetin and DPP-4 (**e**, **f**); the interaction of compounds co-crystal ligand (Prolyl thiazolidine) and DPP-4 (**g**, **h**)

possible efficacy in targeting DPP-4. These results suggest that Cassiaoccidentalin B, Isoorientin and Isoquercetin are potential candidates for DPP-4 inhibition, with Cassiaoccidentalin B showing the most significant binding interactions (Figs. 3(m)-3(o)). Molecular modeling studies serve as an essential tool for discovering potential DPP-4 inhibitors. By modeling the interactions between potential inhibitors and the DPP-4 enzyme, researchers can predict which compounds are likely to bind efficiently and inhibit the enzyme's function. This information is subsequently utilized to direct additional in vitro and in vivo investigations, ultimately facilitating the expedited identification and development of novel antidiabetic drugs.

UV-visible Spectra Analysis

When *M. pudica* ethanol extract was combined with zinc sulfate precursor, a white precipitate developed, indicating the synthesis of ZnONPs with an 86.3% yield. The synthesized ZnONPs were sonicated for 10 min after becoming soluble in deionized water to examine the UV-visible spectra. The UV-visible wavelength range was 200–500 nm. The UV-visible spectra indicated the effective synthesis of ZnONPs, which showed a prominent absorption peak around 360 nm (Fig. 4). The absorption peak of ZnONPs coincides with the synthesized ZnONPs from *Papaver somniferum* L [41]., *Alnus nepalensis* D. Don [42] and *Talaromyces islandicus*-mediated ZnONPs [36]. Our current

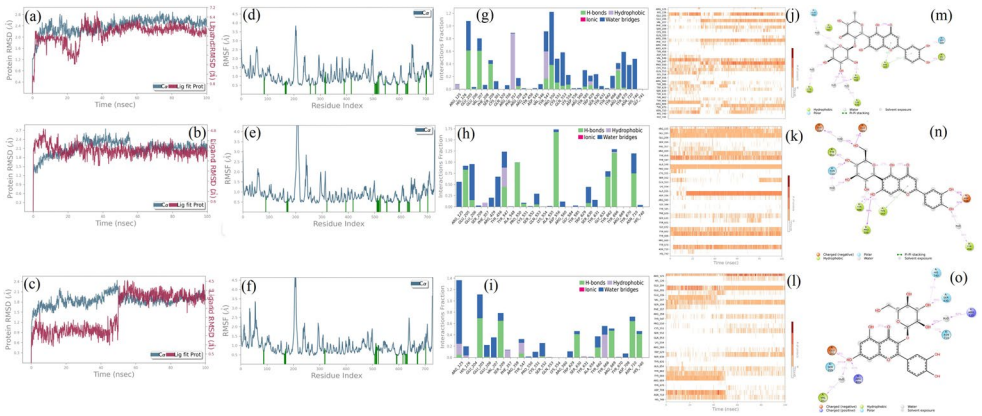

Fig. 3 Plotting the root mean square deviation (RMSD) research for a 100-nanoseconds molecular dynamics (MD) simulation of the docked complex between cassiaoccidentalin B and DPP-4 (**a**), Isoorientin and DPP-4 (**b**), Isoquercetin and DPP-4 docked complex (**c**). Root mean square fluctuation of the cassiaoccidentalin B for characterizing changes in the ligand atom positions (**d**), root mean square fluctuation of the isoorientin for characterizing changes in the ligand atom positions (**e**), root mean square fluctuation of the isoquercetin for characterizing changes in the ligand atom positions (**f**). Percentage of amino acid and water-mediated interactions in MD simulations with cassiaoccidentalin B (**g**), Isoorientin (**h**), Isoquercetin (**i**). The timeline representation of the cassiaoccidentalin B (**j**) DPP-4-cassiaoccidentalin B contacts concerning the amino acids in the target (**m**). The timeline representation of the isoorientin (**k**) DPP-4-isoorientin contacts concerning the amino acids in the target (**n**). The timeline representation of the isoquercetin (**l**) DPP-4-isoquercetin contacts concerning the amino acids in the target (**o**)

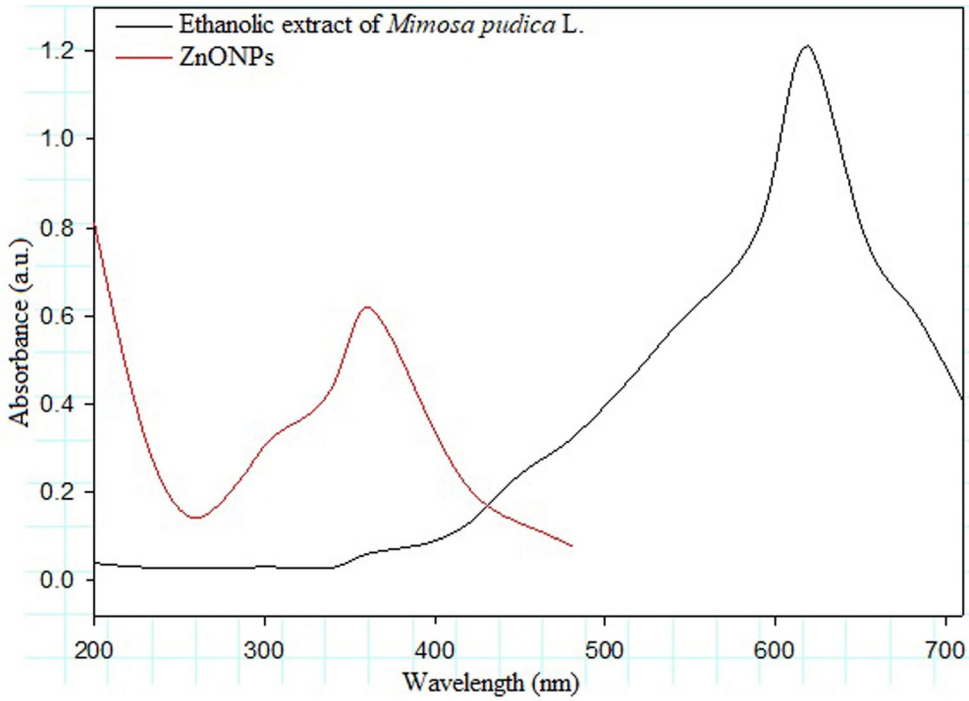

Fig. 4 UV–visible absorption spectra of ethanol extract of *M. pudica*-mediated synthesized ZnONPs and ethanol extract of *Mimosa pudica*

research validated these outcomes. The absorption band that extends to longer wavelengths may result from the movement of the electronic cloud across the ZnONPs framework. UV-visible spectroscopy analysis was conducted on the ethanol extract of *M. pudica*, revealing a peak at a wavelength of 610 nm (Fig. 4). The *M. pudica* extract contains alkaloids, flavonoids, proteins, and antioxidant components, and these compounds act as reducing agents, effectively converting zinc ions (Zn^{2+}) into ZnO. The presence of these compounds in the plant extract could donate the electrons that could reduce zinc metal salt, resulting in the formation of ZnONPs. This study proved that ZnONPs may be generated in massive quantities using chemically comparable plant-mediated production methodologies.

FTIR Analysis

The functional groups in the *M. pudica* extract that could act as reducing agents as well as stabilizing agents during the synthesis of ZnONPs were identified using FTIR spectroscopy. The present study identified that zinc sulfate was reduced into ZnONPs by the bioactive compounds of *M. pudica*. Fig. 5; Table 2 illustrate the FTIR spectral peak and their assignments, signifying the green-synthesized ZnONPs and the ethanol extract from the roots of *M. pudica*. The FTIR spectra of the *M. pudica* extract-mediated synthesized ZnONPs exhibited a broad peak around 3315 cm^{-1}, indicating the stretching and bending vibrations of the −OH group attributable to water adsorption on the metal's surface. The absorption peaks observed at about 2976–2887 cm^{-1} indicated a C–H stretching vibration that might be obtained from plant bioactive compounds. The bioactive components in the plant extract facilitate the reduction of metal

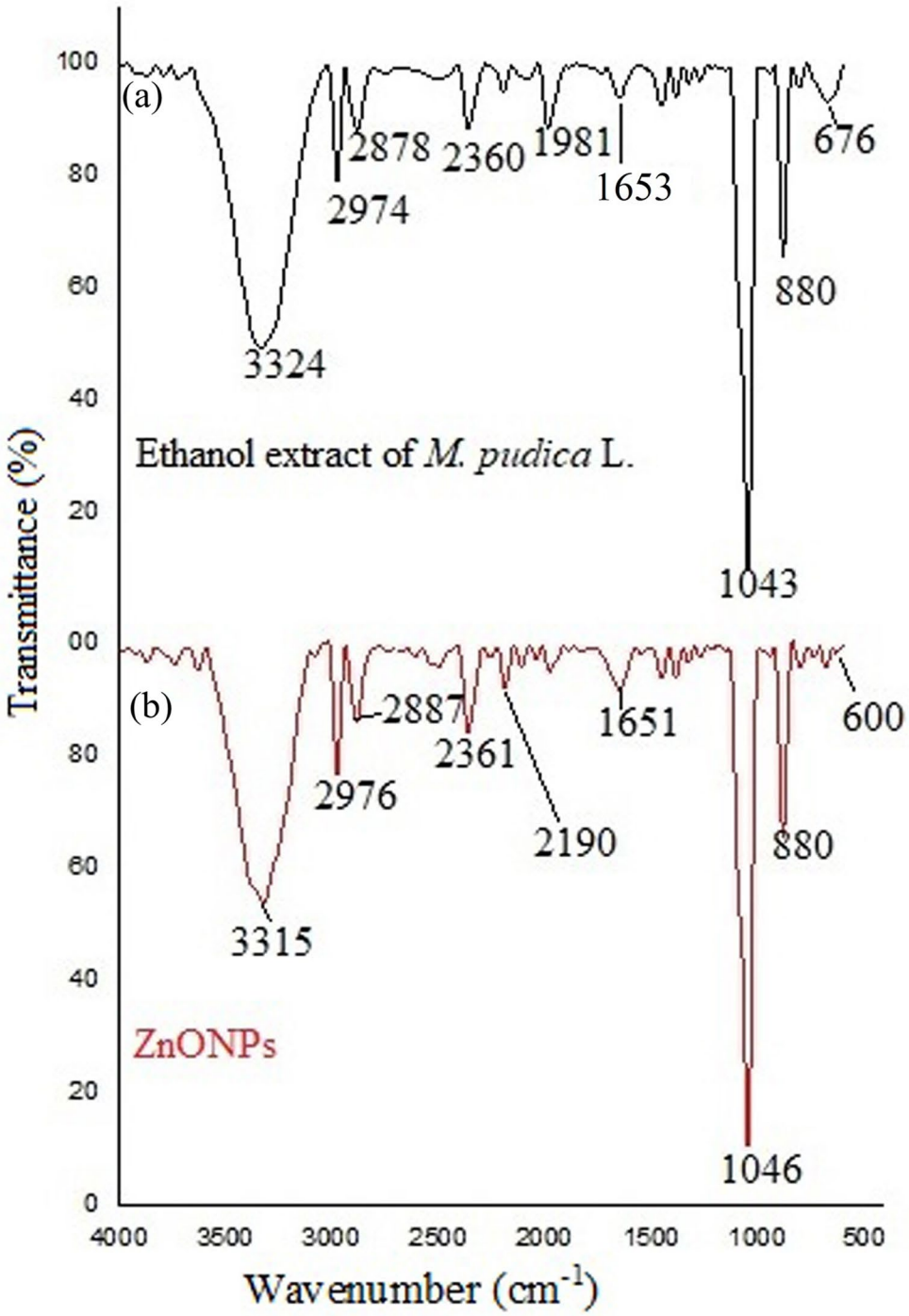

Fig. 5 FTIR spectra of ethanol extract of *M. pudica* (**a**) and biosynthesized ZnONPs (**b**)

Table 2 Positions of FTIR absorption peaks and their functional assignment groups for the ethanol extract of *M. pudica* root and their derived ZnONPs

M. pudica ethanol extract Wavenumber (cm-1)	Assignments	ZnONPs Wavenumber (cm-1)	Assignments
3324	-OH stretching	3315	-OH stretching
2974	-CH stretching vibration	2976	-CH stretching vibration
2878	-CH stretching vibration	2887	-CH stretching vibration
2360	O=C=O stretching	2361	O=C=O stretching
1981	C=C=C stretching	2190	C≡C stretching
1653	Aromatic rings	1651	Aromatic rings
1043	-C-O stretching vibration	1046	-C-O stretching vibration
880	-CH stretching vibration	880	-CH stretching vibration
676	Off-plane deformation vibration	600	Zn-O vibrations

ions into nanoscale structures. On the other hand, the peak displayed at 1651 cm^{-1} corresponds to the stretching vibration properties of aromatic rings. The absorption peaks obtained at 1046 cm^{-1} and 880 cm^{-1} correspond to the C–H in-plane and out-of-plane bending stretching. The peak detected at approximately 600 cm^{-1} signified the stretching vibrations of ZnO. Literature study suggested that C–H, C–O–C, and C=C groups of heterocyclic compounds could have stabilizing properties [43]. The metal (Zinc)-oxygen (ZnO) stretching absorption was often detected in the 400–800 cm^{-1} [44]. These results agree with the FTIR spectra of ZnONPs previously published in various plant extracts [42]. The conversion of zinc ions into zinc oxide nanoparticles and their stabilization in an aqueous medium is ascribed to the bioactive constituents of plant extract, such as phenolic compounds, proteins, and steroids, as indicated by FTIR analysis results [45].

XRD Analysis

The XRD analysis confirmed the crystallinity of the synthesized ZnONPs using an X-ray diffractometer. Fig. 6 displays the XRD pattern of the ethanol extract of *M. pudica* -extract mediated synthesized ZnONPs. The crystallinity of the powder resulted from the synthesis using ethanol extract from *M. pudica.* The diffraction peaks of the synthesized ZnONPs at 2θ values are 18.54°, 21.86°, 26.17°, 35.49°, 54.61°, 58.12°, and 64.13°, likened to planes such as (100), (002), (101), (102), (110), (103), and (112) are lattice planes. The diffraction peaks revealed that the synthesized ZnONPs are essentially crystalline. All prominent diffraction peaks in the XRD spectra corresponded with those documented in the Joint Committee on Powder Diffraction Standards (JCPDS, card No. 89-7102) [46], which confirmed the crystallographic Wurtzite structure [47]. Impurities of diffraction

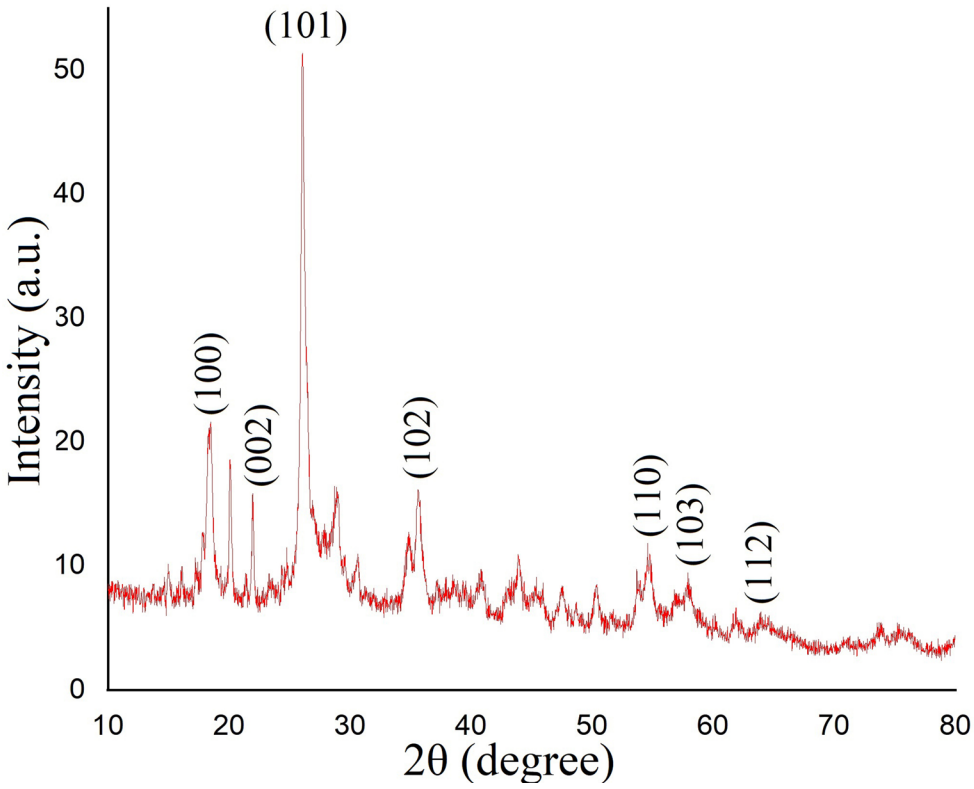

Fig. 6 XRD pattern of lyophilized powder of ZnONPs

peaks were not detected, which proved the high purity of the products. The following Debye–Scherrer equation was used to measure the size of synthesized ZnONPs.

$D = k\lambda/\beta_s \cos\theta$.

D represents the crystallite size, while k is contingent upon size. Debye–Scherrer constant (0.94 for spherical particles), λ represents the wavelength of incident X-radiation (1.548 Å), and βs denotes the full width at half maximum. The mean diameter of the synthesized ZnONPs was ascertained to be 45 nm. The observed size of the ZnONPs is consistent with the report of Shah Faisal et al. 2022 [48]. This discovery is analogous to previously documented dimensions, such as 11.9 nm [49], demonstrating consistency and reliability in the synthesis and characterization methodologies.

Particle Size Analysis

The primary purpose of dynamic light scattering (DLS) analysis is to ascertain the particle sizes in various suspensions. The degree of particle aggregation in aqueous media was evaluated by the mean hydrodynamic particle diameter (d. nm) [50]. The intensity-weighted mean diameter (z-average) and zeta potential of ZnONPs mediated by *M. pudica* extract are determined using DLS, as illustrated in Figs. 7(a) and 7(b). The synthesized ZnONPs exhibit a particle size of around 50 to 100 nm, a polydispersity index of approximately 0.4, with a zeta potential of -0.153 mV. The results indicate that the nanoparticles are highly stable and monodisperse. Our DLS findings for ZnONPs are consistent with previous studies utilizing leaf extracts from *Elaeagnus angustifolia* L. for the synthesis of ZnONPs [51]. The XRD and this result show that the produced ZnONPs have high crystallinity. Since the generated ZnONPs particle size is about 100 nm, it is considered an excellent outcome.

XPS Analysis

Fig. 8 illustrates the high-resolution XPS survey spectra of the ethanol root extract of *M. pudica*-mediated synthesized ZnONPs. The substance's composition was confirmed by the presence of carbon (C 1s), oxygen (O 1s), and nitrogen (N 1s). The survey study confirmed the presence of Zn through Zn (3p, 3d, 3s, LM1, LM2, and LM). The C 1s signal indicates that the C (H, C), C–N, C–O, C=O, and C–O–C groups from *M. pudica* extract phytocompounds exhibit a peak at 288 eV. The O1s peak at 587 eV arises from the–C–O–H group of *M. pudica* extract phytocompounds, while the N1s signal at 534 eV is attributed to the presence of the C–N bond in *M. pudica* extract phytocompounds. Zn exhibits many peaks at 15 eV (Zn 3d), 91 eV (Zn 3p), 114 eV (Zn 3s), 479 eV (Zn LM1), 501 eV (Zn LM2), and 558 eV (Zn LM3). These peaks signify the existence of Zn in the form of Zn (II) oxide [52].

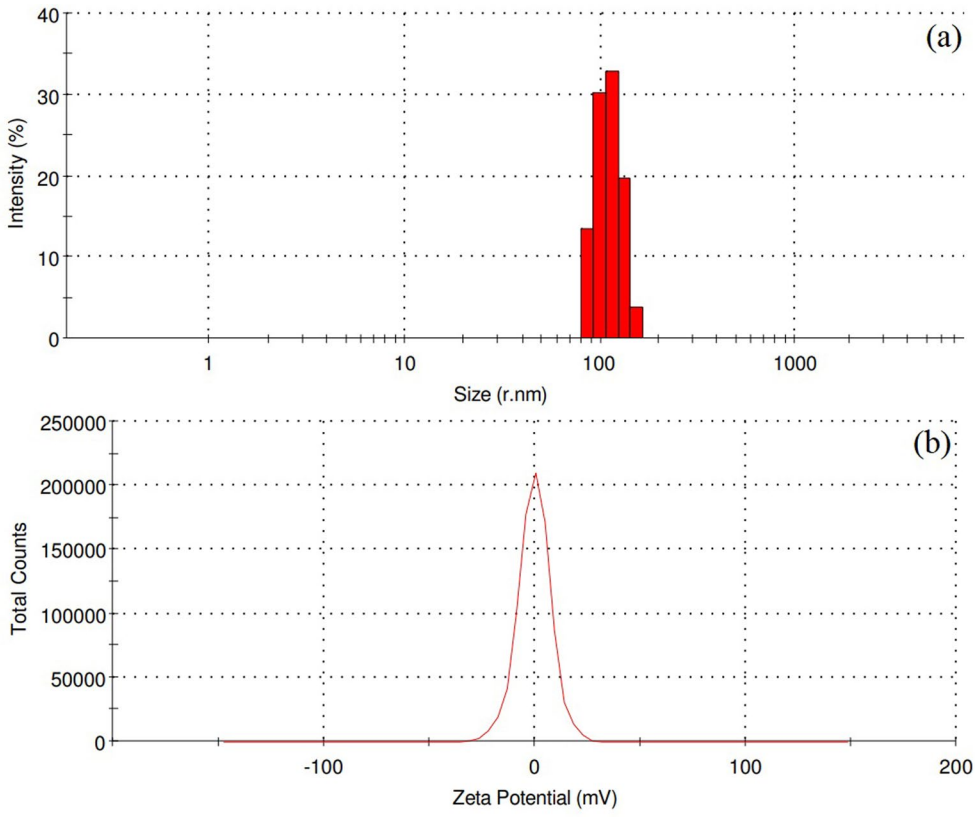

Fig. 7 DLS analysis of the ethanol extract of *M. pudica*-mediated synthesized ZnONPs. Dynamic particle size distribution (**a**), and zeta potential (**b**) of ZnONPs

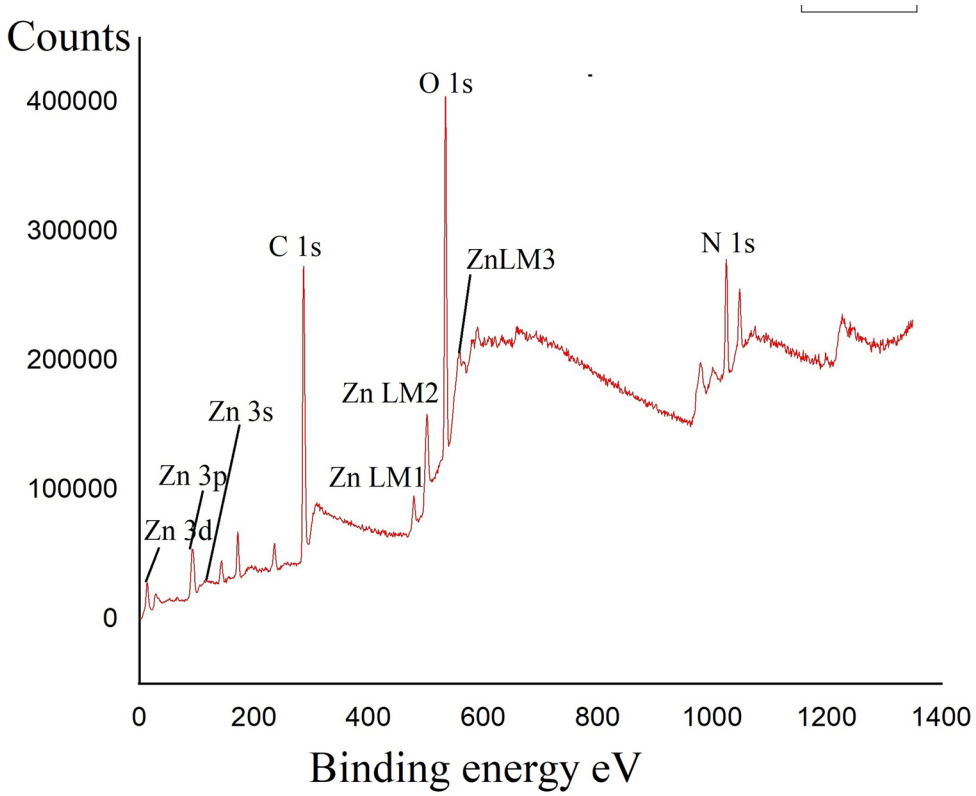

Fig. 8 XPS spectrum of ZnONPs

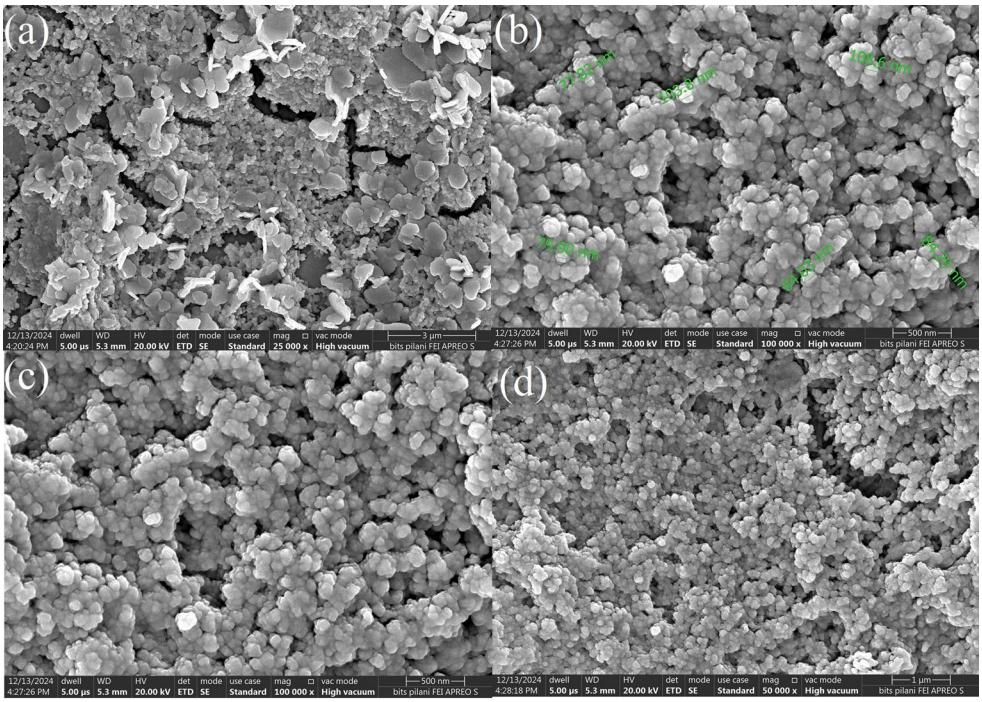

Fig. 9 Field emission scanning electron microscope images of biologically synthesized ZnONPs (**a**)–(**d**)

FESEM and EDAX

FESEM analysis was conducted to examine the dimensions and morphology of ZnONPs. Figs. 9(a)-9(d) illustrate the morphological characteristics at various magnifications and scales of synthesized ZnONPs, predominantly exhibiting a spherical morphology. The average size of ZnONPs was roughly 40 to 100 nm. The elemental composition and chemical analysis of synthesized ZnONPs were assessed using EDAX (Fig. 10(a)). The research examined Zn, O,

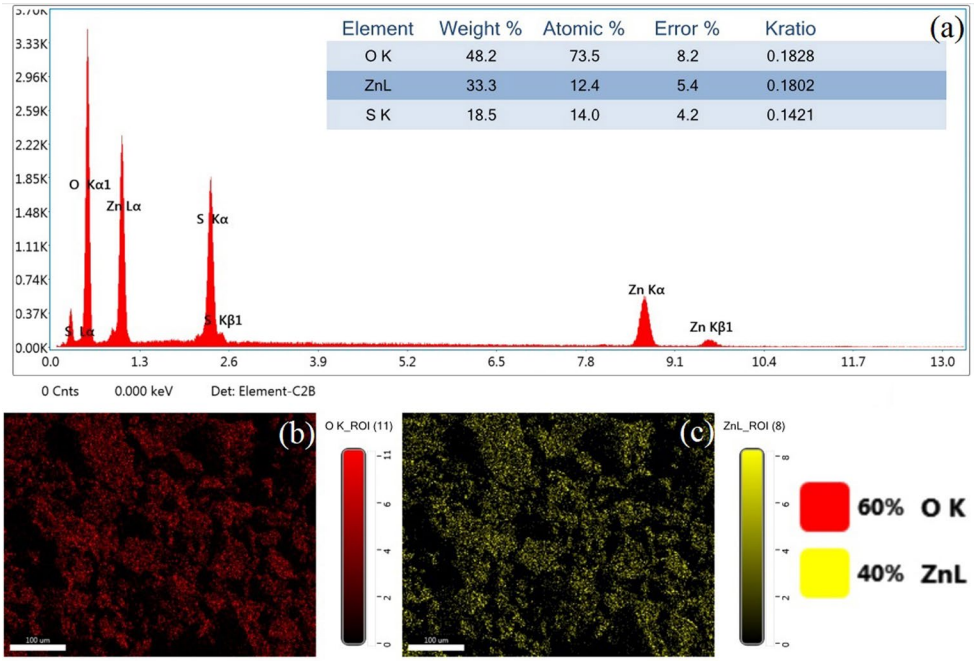

Fig. 10 EDAX pattern of synthesized ZnONPs (**a**), and EDAX elemental mapping of synthesized ZnONPs (**b**) and (**c**)

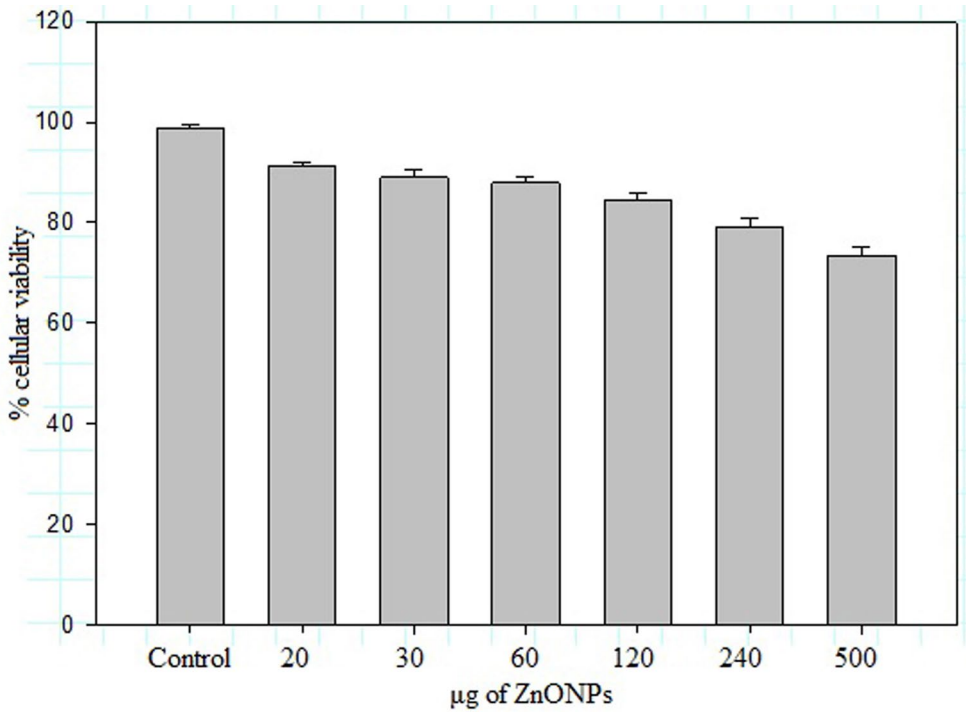

Fig. 11 The ability of cellular viability of synthesized ZnONPs at different concentrations. Data are presented as mean ± standard deviation ($n = 3$ in each group)

and C within the ZnONPs. EDAX mapping revealed around 40% zinc and 60% oxygen (Figs. 10(b) and 10(c)). This study indicates that the presence of carbon signifies the integration of the capping agent in the ZnONPs. The reference indicated a comparable outcome for SEM analysis [53].

Cellular Viability Studies of ZnONPs

The MTT assay determined the in vitro cellular viability against the tested samples. It describes cellular proliferation, viability, and cytotoxicity and tracks how well cells respond to different stimuli following treatment in culture media. The cytotoxic effect of ZnONPs at various concentrations (20, 30, 60, 120, 240, and 500 µg) in 3T3-L1 adipocytes for 24 h is depicted in Fig. 11. The findings showed that the cell

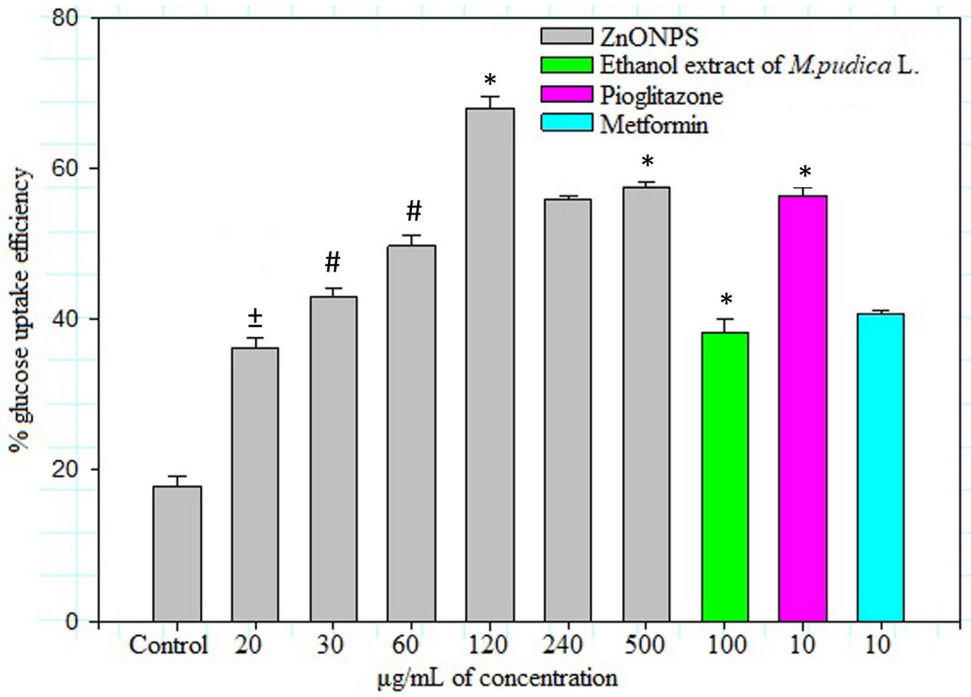

Fig. 12 *In vitro* glucose utilization efficiency of ethanol extract of *M. pudica*-mediated synthesized ZnONPs in 3T3-L1 adipocytes. Data are presented as mean ± standard deviation ($n = 3$ in each group). *$p < 0.01$ as compared to control, ±$p < 0.01$ as compared to metformin and control, #$p < 0.05$ as compared to 60 µg & 60 µg of ZnOPs and control

viability of 3T3-L1 adipocytes declines as the concentration of ZnONPs increases. 3T3-L1 adipocytes may maintain cellular viability at higher ZnONPs concentrations. Therefore, a 500 µg concentration of ZnONPs is primarily responsible for the observed cell viability of 73.47 ± 1.59% on 3T3-L1 adipocytes. Cell viability was observed at 84.56 ± 1.42% at 120 µg ZnONPs. This study proved no cytotoxic effects of *M. pudica* ethanol extract-mediated synthesized ZnONPs. Similarly, no cytotoxic effects were reported by *Cyperus Rotundus* grass extracts-mediated synthesis of zinc oxide nanostructures [54].

In Vitro Glucose Utilization Efficiency of ZnONPs

Using 6-NBDG, the impact of *M. pudica*-extract-mediated ZnONPs on glucose utilization efficiency was measured. Differentiated 3T3-L1 adipocytes were preincubated with the *M. pudica* L. extract (100 µg), varying concentrations of ZnONPs (20, 30, 60, 120, 240 and 500 µg), pioglitazone (10 µg), and metformin (10 µg) for 24 h. In comparison to 100 µg *M. pudica* L. extract (38.28 ± 1.64%), 10 µg pioglitazone (56.32 ± 1.08%), and 10 µg metformin (40.65 ± 0.39%), the adipocytes treated with 120 µg of ZnONPs demonstrated the highest uptake of glucose (6-NBDG) (68 ± 1.55%). 3T3-L1 adipocytes treated with ZnONPs exhibit a dose-dependent rise in glucose absorption, a highly promising finding that can be attributed to the impact of ZnONPs (Fig. 12). Additionally, in 3T3-L1 adipocytes, the effect of glucose uptake on 60 µg of ZnONPs was higher than that of metformin (49.68 ± 1.49%) and comparable to 10 µg pioglitazone (56.32 ± 1.08%). A class of glucose transporter proteins (GLUT4) facilitates glucose uptake in skeletal muscle and adipose tissue. When insulin levels are low, GLUT4 stays lodged in the vesicles [55]. Following its binding to the receptor, insulin phosphorylates the insulin receptor substrate (IRS), which triggers the activation of protein kinase B via a sequence of signaling cascade molecules [56]. As a result, GLUT4 can move from the vesicle to the plasma membrane. As a result, the free glucose diffuses into the cell more easily along its concentration gradient [55]. Numerous plant-derived compounds have been shown to improve glucose translocation and increase the insulin-dependent pathway [57–59]. Enhanced blood glucose levels and enhanced serum DPP-4 activity levels are hallmarks of type 1 and type 2 diabetes. Based on the results of our study, DPP-4 inhibition enhanced GLUT4 expression and membrane insertion, increasing adipocytes' glucose absorption. These DDP-4 inhibitors of *M. pudica* bioactive substances may reduce insulin resistance in the liver or muscle cells. Although plant extract-mediated manufactured ZnONPs show potential in diabetes management, their limitations encompass conflicting findings across research, possible interactions between metal ions and drugs, and the necessity for more rigorous clinical trials to elucidate processes, delivery, and dosing comprehensively. Additionally, the complexity of plant extracts and the possibility for diversity in preparation and extraction procedures might lead to conflicting outcomes.

Conclusion

The research demonstrated that an ethanol extract of *M. pudica* synthesized ZnONPs as an antidiabetic agent, efficiently improving glucose utilization in 3T3-L1 adipocyte cells via inhibiting DPP-4. Biosynthesized ZnONPs showed better glucose utilization efficiency than the *M. pudica* extract and metformin, which may be because nanosized particles can penetrate the cells and modulate their function. The extract, rich in bioactive compounds, facilitates the synthesis of nanosized ZnONPs that effectively infiltrate cells and enhance glucose uptake from the bloodstream. Green-synthesized ZnONPs exhibited non-toxic and cytoprotective properties. Nonetheless, some limitations of the early investigation must be recognized. The primary evident restriction is that the drug's efficacy was not evaluated in animal models. The potential clinical applications of ZnONPs in antidiabetic therapy have established a novel, economical alternative for treating diabetes mellitus. Further, in vivo animal studies are necessary to elucidate the molecular mechanisms responsible for the enhanced glucose utilization in 3T3-L1 adipocyte cells induced by *M. pudica*-mediated synthesized ZnONPs. Future study must investigate their molecular activity, refine nanoformulations, assess long-term safety, and examine therapeutic or pharmacological applications. Connecting in vitro discoveries with in vivo applications will be essential for their effective translation into metabolic health therapies.

Supplementary Information The online version contains supplementary material available at https://doi.org/10.1007/s12247-025-10064-x.

Acknowledgements The authors are grateful to the Management of Sethu Institute of Technology, Kariapatti, Tamil Nadu, India, for providing all required research facilities.

Author Contributions CP and SK contributed to the study's conception and design. CP, PP, PT, MS (4th author), MS (5th author), and SK performed biodistribution studies and computational simulations and analyzed the data. CP and SK wrote the original manuscript. CP, PP, PT, MS (4th author), MS (5th author), and SK proofread the manuscript. All the authors have read and approved the manuscript for submission.

Funding No funding was received for this study.

Data Availability No datasets were generated or analysed during the current study.

Declarations

Ethics Approval and Consent to Participate Not applicable.

Consent for Publication All authors gave their entire consent for publication.

Competing Interests The authors declare no competing interests.

References

1. Mukhtar Y, Galalain A, Yunusa U. A modern overview on diabetes mellitus: a chronic endocrine disorder. Eur J Biol. 2020;5(2):1–14. https://doi.org/10.47672/ejb.409.
2. Abdul Basith Khan M, Hashim MJ, King JK, Govender RD, Mustafa H, Al Kaabi J. Epidemiology of type 2 diabetes-global burden of disease and forecasted trends. J Epidemiol Glob Health. 2020;10(1):107–11. https://doi.org/10.2991/jegh.k.191028.001.
3. Gregory GA, Robinson TI, Linklater SE, Wang F, Colagiuri S, de Beaufort C, Donaghue KC, Harding JL, Wander PL, Zhang X. Global incidence, prevalence, and mortality of type 1 diabetes in 2021 with projection to 2040: a modelling study. Lancet Diabetes Endocrinol. 2022;10(10):741–60. https://doi.org/10.1016/S2213-8587(22)00218-2.
4. Dagenais GR, Gerstein HC, Zhang X, McQueen M, Lear S, Lopez-Jaramillo P, Mohan VP, Mony P, Gupta R, Kutty VR. Variations in diabetes prevalence in low-, middle-, and high-income countries: results from the prospective urban and rural epidemiological study. Diabetes Care. 2016;39(5):780–7. https://doi.org/10.2337/dc15-2338.
5. Galicia-Garcia U, Benito-Vicente A, Jebari S, Larrea-Sebal A, Siddiqi H, Uribe KB, Ostolaza H, Martín C. Pathophysiology of type 2 diabetes mellitus. Int J Mol Sci. 2020;21(17):6275. https://doi.org/10.3390/ijms21176275.
6. Dimitriadis GD, Maratou E, Kountouri A, Board M, Lambadiari V. Regulation of postabsorptive and postprandial glucose metabolism by insulin-dependent and insulin-independent mechanisms: an integrative approach. Nutrients. 2021;13(1):159. https://doi.org/10.3390/nu13010159.
7. Stephens JM, Pilch PF. The metabolic regulation and vesicular transport of GLUT4, the major insulin-responsive glucose transporter. Endocrinol Rev. 1995;16(4):529–46. https://doi.org/10.1210/edrv-16-4-529.
8. Müller T, Finan B, Clemmensen C, DiMarchi R, Tschöp M. The new biology and pharmacology of glucagon. Physiol Rev. 2017;97(2):721–66. https://doi.org/10.1016/j.cmet.2022.10.001
9. Mohammed S, Yaqub A, Sanda K, Nicholas A, Arastus W, Muhammad M, Abdullahi S. Review on diabetes, synthetic drugs and glycemic effects of medicinal plants. J Med Plants Res. 2013;7(36):2628–37. https://doi.org/10.5897/JMPR2013.5169.
10. Boden G. Free fatty acids—the link between obesity and insulin resistance. Endocrinol Pract. 2001;7(1):44–51. https://doi.org/10.4158/EP.7.1.44.
11. Pittas AG, Joseph NA, Greenberg AS. Adipocytokines and insulin resistance. J Clin Endocrinol Metab. 2004;89(2):447–52. https://doi.org/10.1210/jc.2003-031005.
12. Nargis T, Chakrabarti P. Significance of circulatory DPP4 activity in metabolic diseases. IUBMB Life. 2018;70(2):112–9. https://doi.org/10.1002/iub.1709.
13. Jonik S, Marchel M, Grabowski M, Opolski G, Mazurek T. Gastrointestinal incretins—glucose-dependent insulinotropic polypeptide (GIP) and glucagon-like peptide-1 (GLP-1) beyond pleiotropic physiological effects are involved in pathophysiology of atherosclerosis and coronary artery disease—state of the art. Biol. 2022;11(2):288. https://doi.org/10.3390/biology11020288
14. Holst JJ. The incretin system in healthy humans: the role of GIP and GLP-1. Metabolism. 2019;96:46–55. https://doi.org/10.1016/j.metabol.2019.04.014.
15. Michałowska J, Miller-Kasprzak E, Bogdański P. Incretin hormones in obesity and related cardiometabolic disorders: the

clinical perspective. Nutrients. 2021;13(2):351. https://doi.org/10.3390/nu13020351.
16. Ceperuelo-Mallafré V, Duran X, Pachón G, Roche K, Garrido-Sánchez L, Vilarrasa N, Tinahones FJ, Vicente V, Pujol J, Vendrell J. Disruption of GIP/GIPR axis in human adipose tissue is linked to obesity and insulin resistance. J Clin Endocrinol Metab. 2014;99(5):E908–19. https://doi.org/10.1210/jc.2013-3350.
17. Busek P, Duke-Cohan JS, Sedo A. Does DPP-IV Inhibition offer new avenues for therapeutic intervention in malignant disease? Cancers. 2022;14(9):2072. https://doi.org/10.3390/cancers14092072.
18. Kounatidis D, Vallianou NG, Karampela I, Rebelos E, Kouveletsou M, Dalopoulos V, Koufopoulos P, Diakoumopoulou E, Tentolouris N, Dalamaga M. Anti-diabetic therapies and cancer: from bench to bedside. Biomolecules. 2024;14(11):1479. https://doi.org/10.3390/biom14111479
19. Zhang J, Wu N, Shi D. The involvement of the mammalian target of rapamycin, protein tyrosine phosphatase 1b and dipeptidase 4 signaling pathways in cancer and diabetes: a narrative review. Mini Rev Med Chem. 2021;21(7):803–15. https://doi.org/10.2174/1389557520666201113110406.
20. Kambale EK, Katemo FM, Quetin-Leclercq J, Memvanga PB, Beloqui A. Green-synthesized zinc oxide nanoparticles and plant extracts: a comparison between synthesis processes and antihyperglycemic activity. Int J Pharm. 2023;635:122715. https://doi.org/10.1016/j.ijpharm.2023.122715.
21. Nkemzi AQ, Okaiyeto K, Oyenihi O, Opuwari CS, Ekpo OE, Oguntibeju OO. Antidiabetic, anti-inflammatory, antioxidant, and cytotoxicity potentials of green-synthesized zinc oxide nanoparticles using the aqueous extract of helichrysum cymosum. 3 Biotech. 2024;14(12):1–17. https://doi.org/10.1007/s13205-024-04125-0.
22. Khan MI, Shah S, Faisal S, Gul S, Khan S, Abdullah, Shah SA, Shah WA. Monotheca buxifolia driven synthesis of zinc oxide nano material, its characterization and biomedical applications. Micromachines. 2022;13(5):668. https://doi.org/10.3390/mi13050668.
23. Al-Radadi NS, Faisal S, Alotaibi A, Ullah R, Hussain T, Rizwan M, Zaman N, Iqbal M, Iqbal A, Ali Z. *Zingiber officinale* driven bioproduction of ZnO nanoparticles and their anti-inflammatory, anti-diabetic, anti-Alzheimer, anti-oxidant, and anti-microbial applications. Inorg Chem Commun. 2022;140:109274. https://doi.org/10.1016/j.inoche.2022.109274.
24. Nilavukkarasi M, Vijayakumar S, Prathipkumar S. *Capparis Zeylanica* mediated bio-synthesized ZnO nanoparticles as antimicrobial, photocatalytic and anti-cancer applications. Mater Sci Energy Technol. 2020;3:335–43. https://doi.org/10.1016/j.mset.2019.12.004.
25. Dey S, lochan Mohanty D, Divya N, Bakshi V, Mohanty A, Rath D, Das S, Mondal A, Roy S, Sabui R. A critical review on zinc oxide nanoparticles: synthesis, properties and biomedical applications. Intell Pharm. 2024. https://doi.org/10.1016/j.ipha.2024.08.004.
26. Ughade M, Chaudhary PH, Burange PJ, Baig A, Pawar D, Warhekar T, Deshmukh V, Darokar P. A comprehensive review on *Mimosa pudica* Linn. Int Res J Mod Eng Technol Sci. 2025;6(12):2582–5208.
27. Muhammad G, Hussain MA, Jantan I, Bukhari SNA. *Mimosa pudica* L. is a high-value medicinal plant that is a source of bioactives for pharmaceuticals. Compr Rev Food Sci Food Saf. 2016;15(2):303–15. https://doi.org/10.1111/1541-4337.12184.
28. Kaur J, Sidhu S, Chopra K, Khan M. Protective effect of *Mimosa pudica* L. in an L-arginine model of acute necrotising pancreatitis in rats. J Nat Med. 2016;70:423–34. https://doi.org/10.1007/s11418-016-0991-3.
29. Patel P, Garala K, Singh S, Prajapati BG, Chittasupho C. Lipid-based nanoparticles in delivering bioactive compounds for improving therapeutic efficacy. Pharmaceuticals. 2024;17(3):329. https://doi.org/10.3390/ph17030329.
30. Lavanya L, Veeraraghavan V, Srihari R, Prashantha C. Study of *in vitro* activity on glucose uptake of 3T3-L1 cells, RIN5f cells, and glycemic index stimulation inhibitory effect of abutilon indicum (L.) extract. J Appl Biol Biotechnol. 2022;10(1):145–56. https://doi.org/10.7324/JABB.2021.100118.
31. Vilkhu K, Mawson R, Simons L, Bates D. Applications and opportunities for ultrasound assisted extraction in the food industry—A review. Innov Food Sci Emerg Technol. 2008;9(2):161–9. https://doi.org/10.1016/j.ifset.2007.04.014.
32. Halgren TA, MMFF VII. Characterization of MMFF94, MMFF94s, and other widely available force fields for conformational energies and for intermolecular-interaction energies and geometries. J Comput Chem. 1999;20(7):730–48. https://doi.org/10.1002/(SICI)1096-987X(199905)20:7%3C730::AID-JCC%3E3.0.CO;2-T
33. Pardhi E, Tomar DS, Khemchandani R, Bazaz MR, Dandekar MP, Samanthula G, Singh SB, Mehra NK. Monophasic coamorphous sulpiride: a leap in physicochemical attributes and dual Inhibition of GlyT1 and P-glycoprotein, supported by experimental and computational insights. J Biomol Struct Dyn. 2025;43(8):4297–326. https://doi.org/10.1016/j.ijpharm.2024.125056.
34. Lippert RA, Predescu C, Ierardi DJ, Mackenzie KM, Eastwood MP, Dror RO, Shaw DE. Accurate and efficient integration for molecular dynamics simulations at constant temperature and pressure. J Chem Phys. 2013;139(16). https://doi.org/10.1063/1.4825247.
35. Beig B, Niazi MBK, Jahan Z, Haider G, Zia M, Shah GA, Iqbal Z, Hayat A. Development and testing of zinc sulfate and zinc oxide nanoparticle-coated Urea fertilizer to improve N and Zn use efficiency. Front Plant Sci. 2023;13:1058219. https://doi.org/10.3389/fpls.2022.1058219.
36. Sangeeta M, Tejashree, Gunagambhire VM, Bhat MP, Nagaraja SK, Gunagambhire PV, Kumar RS, Mahalingam SM. In-vitro evaluation of *Talaromyces Islandicus* mediated zinc oxide nanoparticles for antibacterial, anti-inflammatory, bio-pesticidal and seed growth promoting activities. Waste Biomass Valori. 2024;15(3):1901–15. https://doi.org/10.1007/s12649-023-02386-z.
37. Vijayakumar S, Pandidurai S, Wadaan MA, Mythili R, Santhosh D, Balamurali N, Vidhya E. ZnO nanoparticles: A sustainable fabrication enhanced by eggshell waste and its germicidal, antiproliferative, and photodecomposition properties. Polym Adv Technol. 2024;35(3):e6353. https://doi.org/10.1002/pat.6353.
38. Kumar S, Kumar V, Bansal MK, Mishra A. Green method production of ZnO nanoparticles using the weed *Ageratum conyzoides* and their antibacterial potential. Results Chem. 2024;12:101909. https://doi.org/10.1016/j.rechem.2024.101909.
39. Pinho AR, Martins F, Costa MEV, Senos AM, da, Cruz e Silva OA, Pereira ML, Rebelo S. *In vitro* cytotoxicity effects of zinc oxide nanoparticles on spermatogonia cells. Cells. 2020;9(5):1081. https://doi.org/10.3390/cells9051081
40. DiNuzzo M, Giove F, Maraviglia B, Mangia S. Glucose metabolism down-regulates the uptake of 6-(N-(7-nitrobenz-2-oxa-1, 3-diazol-4-yl) amino)-2-deoxyglucose (6-NBDG) mediated by glucose transporter 1 isoform (GLUT 1): theory and simulations using the symmetric four-state carrier model. J Neurochem. 2013;125(2):236–46. https://doi.org/10.1111/jnc.12164.
41. Muhammad W, Ullah N, Haroon M, Abbasi BH. Optical, morphological and biological analysis of zinc oxide nanoparticles (ZnO NPs) using *Papaver somniferum* L. RSC Adv. 2019;9(51):29541–8. https://doi.org/10.1039/C9RA04424H.

42. Jaishi DR, Ojha I, Bhattarai G, Baraili R, Pathak I, Ojha DR, Shrestha DK, Sharma KR. Plant-mediated synthesis of zinc oxide (ZnO) nanoparticles using *Alnus Nepalensis* D. Don for biological applications. Heliyon. 2024;10(20). https://doi.org/10.1016/j.heliyon.2024.e39255.
43. Udayagiri H, Sana SS, Dogiparthi LK, Vadde R, Varma RS, Koduru JR, Ghodake GS, Somala AR, Boya VK, Kim SC, Karri RR. Phytochemical fabrication of ZnO nanoparticles and their antibacterial and anti-biofilm activity. Sci Rep. 2024;14(1):19714. https://doi.org/10.1038/s41598-024-69044-9.
44. Gomathi R, Suhana H. Green synthesis, characterization and antimicrobial activity of zinc oxide nanoparticles using *Artemisia pallens* plant extract. Inorg Nano-Met Chem. 2021;51(12):1663–72. https://doi.org/10.1080/24701556.2020.1852256.
45. Selim YA, Azb MA, Ragab I, Abd El-Azim HM. Green synthesis of zinc oxide nanoparticles using aqueous extract of *Deverra tortuosa* and their cytotoxic activities. Sci Rep. 2020;10(1):3445. https://doi.org/10.1038/s41598-020-60541-1.
46. File PD, Kabekkodu S. International centre for diffraction data: Newtown square. USA: PA; 2007.
47. Zhou J, Zhao F, Wang Y, Zhang Y, Yang L. Size-controlled synthesis of ZnO nanoparticles and their photoluminescence properties. J Lumin. 2007;122:195–7. https://doi.org/10.1016/j.jlumin.2006.01.089.
48. Faisal S, Abdullah, Rizwan M, Ullah R, Alotaibi A, Khattak A, Bibi N, Idrees M. *Paraclostridium benzoelyticum* bacterium-mediated zinc oxide nanoparticles and their in vivo multiple biological applications. Oxid Med Cell Longev. 2022;2022(1):5994033. https://doi.org/10.1155/2022/5994033.
49. Talam S, Karumuri SR, Gunnam N. Synthesis, characterization, and spectroscopic properties of ZnO nanoparticles. Int Sch Res Notices. 2012;2012(1):372505. https://doi.org/10.5402/2012/372505.
50. Qiao H, Wei Z, Yang H, Zhu L, Yan X. Preparation and characterization of NiO nanoparticles by anodic Arc plasma method. J Nanomater. 2009;2009(1):795928. https://doi.org/10.1155/2009/795928.
51. Iqbal J, Abbasi BA, Yaseen T, Zahra SA, Shahbaz A, Shah SA, Uddin S, Ma X, Raouf B, Kanwal S. Green synthesis of zinc oxide nanoparticles using *Elaeagnus angustifolia* L. leaf extracts and their multiple *in vitro* biological applications. Sci Rep. 2021;11(1):20988. https://doi.org/10.1038/s41598-021-99839-z.
52. El-Belely EF, Farag MM, Said HA, Amin AS, Azab E, Gobouri AA, Fouda A. Green synthesis of zinc oxide nanoparticles (ZnO-NPs) using *Arthrospira platensis* (Class: Cyanophyceae) and evaluation of their biomedical activities. Nanomater. 2021;11(1):95. https://doi.org/10.3390/nano11010095.
53. Ismail SMM, Ahmed SM, Abdulrahman AF, AlMessiere MA. Characterization of green synthesized of ZnO nanoparticles by using *Pinus brutia* leaves extracts. J Mol Struct. 2023;1280:135063. https://doi.org/10.1016/j.molstruc.2023.135063.
54. Alatawi FS. The potential effect of green synthesis of zinc oxide nanostructures using *Cyperus rotundus* grass extracts on the genes associated with obesity in the 3T3-L1 cell line. J Drug Deliv Sci Technol. 2023;87:104792. https://doi.org/10.1016/j.jddst.2023.104792.
55. Wang T, Wang J, Hu X, Huang X-J, Chen G-X. Current Understanding of glucose transporter 4 expression and functional mechanisms. World J Biol Chem. 2020;11(3):76. https://doi.org/10.4331/wjbc.v11.i3.76.
56. Boura-Halfon S, Zick Y. Phosphorylation of IRS proteins, insulin action, and insulin resistance. Am J Physiol Endocrinol Metab. 2009;296(4):E581–91. https://doi.org/10.1152/ajpendo.90437.2008.
57. El-Nashar HA, Mostafa NM, El-Shazly M, Eldahshan OA. The role of plant-derived compounds in managing diabetes mellitus: a review of literature from 2014 to 2019. Curr Med Chem. 2021;28(23):4694–730. https://doi.org/10.2174/0929867328999201123194510.
58. Naveen J, Baskaran V. Antidiabetic plant-derived nutraceuticals: a critical review. Eur J Nutr. 2018;57:1275–99. https://doi.org/10.1007/s00394-017-1552-6.
59. Manukumar H, Shiva Kumar J, Chandrasekhar B, Raghava S, Umesha S. Evidences for diabetes and insulin mimetic activity of medicinal plants: present status and future prospects. Crit Rev Food Sci Nutr. 2017;57(12):2712–29. https://doi.org/10.1080/10408398.2016.1143446.